 FDMP, vol.4, no.2, pp.77-83, 2008

Numerical and Experimental Study of Particle Motion in Plasma Arc Welding

Adeline Tchikango Siagam[1], Gunther Brenner[1], Peter Giese[2] and Volker Wesling[2]

Abstract: The PTA ("Plasma-Transferred-Arc") is a widespread variant of plasma powder processes to manufacture coatings against corrosion or abrasion. For the optimization of this technique, an explanation of the processes which lead to a maximal deposition performance (i.e. maximal quantity of powder converted per time) is required. Especially the gas and particle flow in the region between the burner nozzle and the work piece is of interest. In the present study, flow simulations (Computational Fluid Dynamics, CFD) have been done in order to investigate the determining factors for the dimensioning of the processes. Additionally, velocity measurements have been obtained with PIV (Particle Image Velocimetry) to validate the computations. This measurement method enables on the one hand the acquisition of the velocity in the gas-phase. On the other hand the velocity of the dispers particle flow can be examined. Due to the high intensities of the plasma light, a modified PIV setup has been used in the present analysis. Comparisons between numerical and experimental results show a good agreement of the velocity fields for large particles. In order to examine simultaneously powder made of particles of different sizes, which are common used in practice, a modified postprocessing based on the classification of the scattered light in different intensity ranges should be taken into consideration.

Keyword: plasma arc welding, PIV, coating

[1] Institute of Applied Mechanics, Clausthal University of Technology, Adolph-Römer-Straße 2A, 38678 Clausthal-Zellerfeld, Email: tchikango@itm.tu-clausthal.de

[2] Institute of Welding and Machining, Clausthal University of Technology, Agricola Straße 2, 38678 Clausthal-Zellerfeld

1 Introduction

PTA ("Plasma-Transferred-Arc") is a thermal coating process which is used to prevent materials from corrosion or abrasion. In this process, additional material is molten and deposited on the surface of the basic material. In the first applications of this kind, the additional material was avalaible as wire or band. Nowadays the introduction of the additional material as powder allows alloys to be used, which can not be formed as wire or band. Furthermore through the use of powder, the thermal burden is reduced.

The powder is ideally fed through a ring nozzle, and two up to four four separate channels are used.

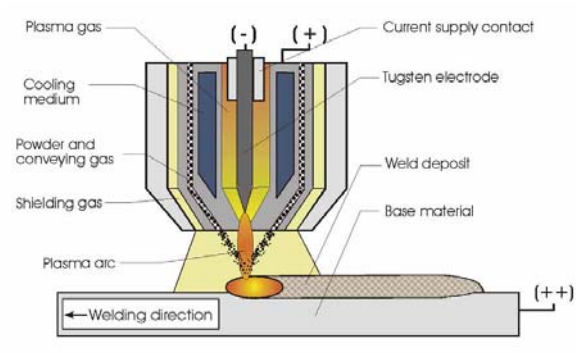

Figure 1: A PTA device

In the process, a plasma light arc is used to melt the powder. In order to shield the process from atmospheric influences, especially oxidation, a shield gas is used. High energy densities are assured through a cylindrical guidance of the plasma arc which in turn is obtained by using a water-cooled nozzle. To optimize PTA processes, a good quality of the weld has to be assured for a large width of energy intensity and powder flow

rate. Former works have shown that the quality of the weld depends on the thermal state of the particles when they reach the substrate, Ansar (2004). The thermal state of the particles depends in turn on their residence time in the plasma and the heat transfer between the particles and the gas. Thus, in order to be able to quantify the process, the velocity distribution of the gasflow and of the particles is of primary interest.

In the early stages of the investigation of the phenomena taking place in the PTA process, statements about the particle flow could have been done via the gas flow, using a balance of the forces acting on the particles. For this purpose the gas velocity was determined over enthalpy probes or dynamic pitot probes, as presented in the work of Jankovic (1997). With the improvement of optical measurements techniques, direct measurement of particle velocity have been enabled. Some of them like the Laser-2-Focus anemometry (L2F) (see Kucuk, Lima, and Berndt (2001)) or the Laser Doppler Velocimetry (LDV) are incorporated in online-diagnosis-systems. With the use of two-wavelength pyrometers, the simultaneous determination of temperature, particle size and particle velocity is enabled, Vardelle, Vardelle, Fauchais, and Moreau (1994). The Particle Image Velocimetry (PIV) has also been successfully used to determine the velocity of the particles in the PTA process (see Zscheztsche, Füssel, Schnick, Zosel, Guth, and Dörner (2005), Bach, Möhwald, Rothardt, Prehm, Engl, Hartz, and Drößler (2004)). In contrast to the other measurements techniques mentioned above, the PIV enables a field measurement of the velocity.

In order to investigate the sensitivity of the operating conditions with respect to the welding result numerical simulation may be used. CFD (Computational Fluid Dynamics) calculations are performed based on the approximate solution of the Reynolds-averaged Navier Stokes equations for a turbulent flow using the finite volume technique.

The scope of this work is to examine the particle flow in the region between burner and work piece using PIV and CFD. In the following section the mathematical model as well as the experimental setup are presented. After this the results will be compared and discussed.

2 Modelling and simulation

The simulation of the powder flow throughput in a PTA burner can be split into two tasks: the simulation of the pure gas flow and the simulation of the powder transport in the gas flow using Euler-Lagrange approach. Thus, the gas flow is modeled on the base of conservation equations of mass, momentum and energy in a fixed or Eulerian reference frame. For a compressible fluid these equations read

$$\frac{\partial \rho}{\partial t} = -\nabla(\rho \mathbf{v}), \tag{1}$$

$$\frac{\partial \rho \mathbf{v}}{\partial t} = -\nabla(\rho \mathbf{v}\mathbf{v}) - \nabla\tau - \nabla p + \rho \mathbf{g}, \tag{2}$$

$$\frac{\partial}{\partial t}(\frac{1}{2}\rho \mathbf{v}^2 + \rho u) = -\nabla\cdot(\frac{1}{2}\rho \mathbf{v}^2 + \rho u)\mathbf{v} - \nabla\dot{\mathbf{q}} - (\nabla\cdot p\mathbf{v}) - (\nabla\cdot|\tau\cdot\mathbf{v}|) + \rho(\mathbf{v}\cdot\mathbf{g}) \tag{3}$$

Equation (1) represents the conservation of mass and eq. (2) balances the rate of change of linear momentum with the change of momentum due to convection, viscous stresses, pressure forces and gravity forces. The viscous forces are obtained for a compressible, Newtonian fluid (see Byron (2002)). The effect of turbulent fluctuations is modelled via an eddy viscosity which is obtained from a k-ε model. In the energy equation (3), the rate of change of total energy due to convection, viscous dissipation, forces and heat conduction is modelled.

The motion of discrete particles is modelled on the base of Newtons law in a Lagrangian or particle fixed frame or reference, i.e.

$$\frac{d\mathbf{x}_p}{dt} = \mathbf{v}_p, \tag{4}$$

$$m_p\frac{d\mathbf{v}_p}{dt} = \Sigma F, \tag{5}$$

$$I_p\frac{d\omega_p}{dt} = \mathbf{T} \tag{6}$$

These equations describe the displacement of particles (4), the change of linear momentum due to

forces acting on the particles (5) and the rate of change of rotational momentum (6). In eqs. (5) and (6), besides the hydrodynamic forces such as lift and drag acting on the particles, gravity, electrosatic and magnetic effects have to be taken into account. The determination of the electrostatics and magnetic forces requires the calculation of the electric and magnetic fields which is subjected of the MHD (Magnetohydrodynamics) module of the present simulation tool (Fluent). Here, Maxwell's equations are used to describe the electromagnetic fields (see FLUENT (2005)).

The computational model presented above represents a system of partial differential equations of second order that are solved in an approximative way using the finite volume method. In addition to the transfer of momentum the program calculates the exchange of heat and mass (vaporization) between discrete and continuous phases. The current simulation uses FLUENT's standard "laws" for the transfer which work sufficiently well for the momentum exchange — the heat transfer will be examined in a different model. Further details of the hydrodynamic model may be found in FLUENT (2005).

Various models for the description of the entire arc physics have already been published, but they are, with very few exceptions (Gonzales, Lago, Freton, Masquere, and Franceries (2005)) mostly limited to two-dimensional solutions or a very narrow sector. Thus, these models are based on the assumption that the system is axissymetric. Particularly the large, steep gradients of temperature and current density close to the electrode tip require an extreme mesh refinement and the system of equations for a three-dimensional model is in this case beyond the scope of single processors machines.

In order to examine the suitability of a three dimensional model, Fig. 2, which has been successfully used for the calculation of gas flows during the welding process, the current density $\mathbf{j}$ was introduced as an additional boundary condition.

This parameter is calculated beforehand from the current of the process, the geometry of the nozzle and the distance between the welding torch and the plate and is then used to calculate the resistance heating

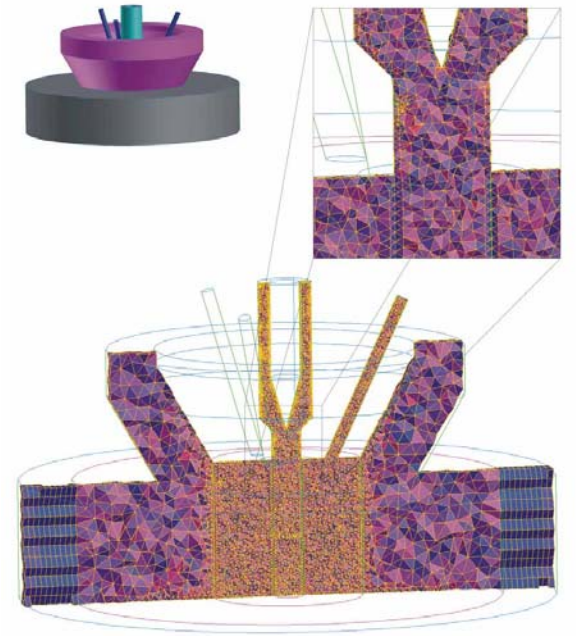

Figure 2: Mesh for the simulation

$$S_h = \frac{j^2}{\sigma}, \tag{7}$$

and the Lorentz force

$$\mathbf{f} = \mathbf{j} \times \mathbf{B} \tag{8}$$

The real current simulation is highly non-uniform and leads to numerical instabilities when used unaltered with the 3D-mesh depicted in Fig. 2. Therefore the extreme maximum near the electrode tip was reduced, the steep gradients were flattened and the overall function approximated by a linear distribution. These terms are then included as an additional source term into the equations of transport by means of user defined functions.

The material data for argon, that has been used as process gas (3,5 l/min), carrier gas (7 l/min) and shield gas (20 l/min) were given for temperatures up to 30000K, Boulos (1994), Murphy and Arundelli (1994). For the simulation of the metal powder spherical particles have been used, whereupon the particle diameters have been defined either as single values or by using real particle size distribution (Rosin-Rammler-distribution). To determine the position and the velocity of the particles,

they are monitored for maximal 500 steps through the model. Interactions with the fluid and gravitation are considered, while effects of electromagnetic interactions as well as effects from the heating up of particles up to melting/vaporizing, as well as repercussion of the metal vapor on the arc have been neglected. The model for the burner and the process region contained about 900.000 cells. Comparative computations with a 2.5 million cells model don't show a significant difference.

3 Experimental Setup

The scope of this part of the work is the determination of the particle velocity in the region between the nozzle and the workpiece. The measurement principle is based on a dual exposure of tracer particles along a light sheet, which are given to the flow. An evaluation of the shift between the particles for the two exposures through a correlation analysis gives the velocity vector field. In order to determine the velocity of the continous phase, i.e. of the gas, it is necessary to use very small particles, to minimize the slip between particles and gas.

The measurements have been fulfilled with a ILA-PIV-System. The coating powder has been used as seeding and the particles were exposed with a dual pulsed Nd:YAG-laser with an energy of 30 mJ and pulse width between 3 and 5 ns. The scattered light is grabbed by a CCD-camera as particles pattern. A particularity of such cameras is that they are able to grab two consecutive pictures in a very short time (e.g. 10 frames per second). In contrast to the first picture, the exposure time of the second picture can not be limited. Because of the high light intensities which occur during the PTA, the second picture will be overexposed and therefore useless. A possible solution is the use of an electro-optical shutter or a second PIV camera. On this way, an optimal setting of the delay and exposure time can be chosen, Zscheztsche, Füssel, Schnick, Zosel, Guth, and Dörner (2005). In this work, a second camera has been used and the experimental setup is sketched in Fig. 3.

The measurement section is made of a 3x3 cm region between nozzle and welding drum. The coating material is conveyed in a gas flow to the burner nozzle and is used as seeding. The injection of the coating material on a turning welding drum avoids that the nozzle and the measurement section have to be moved. 50 mm-lenses have been used and have been connected to the camera with a Scheimpflug mount. In order to avoid noise and to protect the CCD-chips, a band-pass filter for the wave length 532 nm $\pm$ 2 nm and a heat filter are used. The latter is made of Schott KG-1 glass which absorbs IR-radiations and can also be used as a shortpass filter.

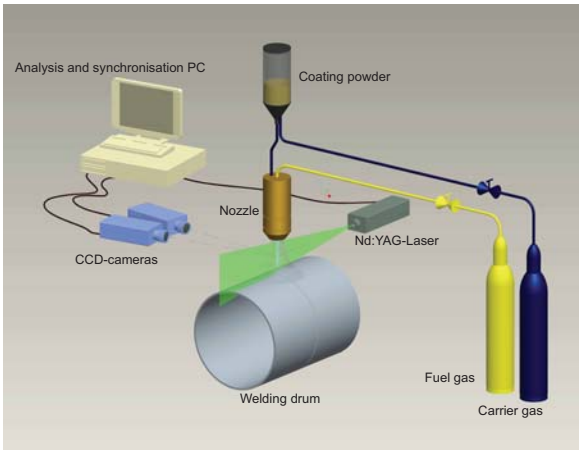

Figure 3: Experimental setup

During a calibration phase, the stereoscopic arrangement of the cameras is optimized. Remaining aberrations are removed by determining an artificial velocity field, that arises from the different positions of a particle pattern on exposures made with the two cameras, and substracting this velocity field from the measured ones. In a further step the delay and exposure time of the camera are chosen. By doing this the pumping time of the laser is considered. For this experimental setup, an optimal pulstime of 75 μs has been established. According to the laser output curve, the laser reaches its maximal power at a frequency between 2 and 5 Hz after a time span of about 160 μs. This is why the first camera will grab the first picture just after 160 μs, when the incoming light quantity is maximal. The exposure time takes 10 μs. Accordingly, the delay time of the second camera lasts 235 μs. The settings are the

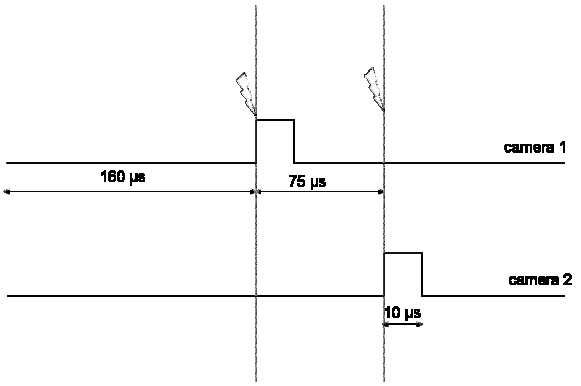

Figure 4: Settings of delay and exposure times

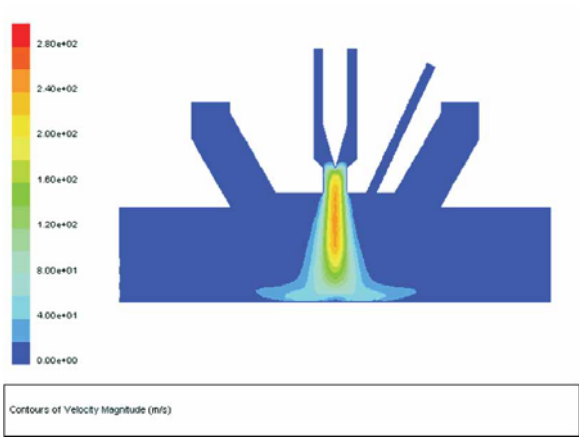

Figure 5: Gas velocities

same for both laser beams. An explaining sketch is given in Fig. 4.

4 Results and discussion

Customary powders for the coat welding consists usually of particles of different sizes. For the commercial mixture Alloy 625, the size distribution ist between 63-200 μm. This particle size distribution is tuned for manufactury purposes and is often determined in laborious experiments. Numerical simulation provides for several grain diameters clearly varied velocities as well as different trajectories for the single particles. Fig. 5 shows the velocity of the argon gas in the plasma column while Fig. 6 shows the simulated flight trajectory for particles with a diameter of 63 μm, 100 μm, and 200 μm respectively, whereupon a defined spreading has been prescribed at the outlet of the nozzle.

From this picture, it can be seen that the particles show the highest velocities close to the center, in the region of the light arc, while on the external trajectories lower velocities are reached. Fig. 7 shows the maximal velocities (z-component) for small and big particles.

The highest values correspond to the particles which flow trough the center of the plasma column. The values of 20 m/s found here for small particles and 7 m/s for big particles can be confirmed by the analysis of exposures made with a high speed camera (see Wesling and Giese (2006)). The lower values inside a size category

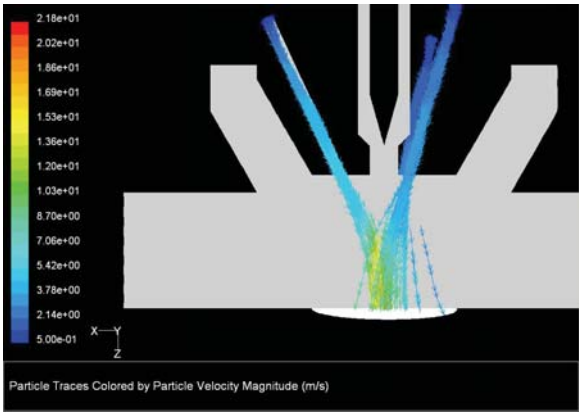

Figure 6: Simulated trajectory for particles with a diameter d_p = 200 μm, d_p = 100 μm and d_p = 63 μm

correspond to the outer flying particles. Exposures made with a high-speed camera show that maximal reached velocities also tend to decrease in the outer regions. However, neither an accurate quantitative analysis nor an exact localisation of the particles is possible. In lieu thereof, Particle Image Velocimetry measurements are an alternative to provide the total velocity distribution in a plane.

Velocity measurements have been done for the mixture Alloy 625, for which the maximal particle diameter adds up to 200 μm. Despite a slight adjustment of the cameras to each other, a relative good accordance with the results of the numerical simulation is observed. In Fig. 8, it can be seen that the maximal reached velocity is about 7 m/s,

as expected from the simulation in Fig. 7. Because velocities up to 20 m/s are reached for particles of the diameter 63 μm, according to Fig. 7, it can be concluded that smaller particles, which show high velocities, are not captured during the PIV measurements. This is because intensity of the scattered light depends on the size of the particles and in this case the small particles do not scatter enough light to be highlighted.

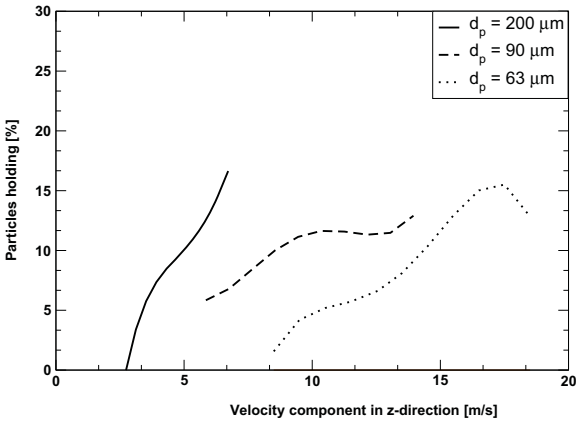

Figure 7: Computed distribution of the velocity-component in z-direction for d_p = 200 μm, d_p = 90 μm, d_p = 63 μm

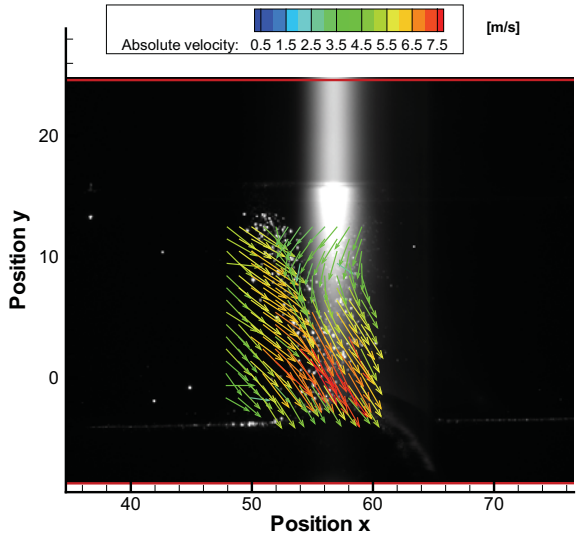

Figure 8: PIV-measurement of the velocity field for the particle mixture Alloy 625

5 Conclusion

In this work, the particle flow during the welding process in a PTA-device has been examined using numerical and experimental methods. Due to the modified PIV-setup, the particle flow by burning plasma could be visualised and investigated. A comparison with results from numerical simulation shows a good agreement between the computed and the measured velocities. However, the measured velocity field is mainly determinated by the bigger particles. The sensitivity of the PIV-setup to possible vibrations or shocks during the measurement is considerably notable for a stereoscopic setup and can be reduced in the future by using a beam splitter (see Zscheztsche, Füssel, Schnick, Zosel, Guth, and Dörner (2005)). Because polydispers particle compounds are often used in welding processes, the PIV-method should be further developed, so that a as wide as possible particle size distribution can be investigated. For this purpose, the light intensities could be split in several ranges, and accordingly a separated analysis should be done, as shown from Ikeda, Yamada, and Nakajima (2000) for velocity measurements during a plasma spraying process. While the current simulation focuses solely on the particle velocities, it already calculates the particle temperatures as a byproduct. This part needs to be addressed in an expanded modell that includes the simulation of the weld pool, thus allowing to examine the overall energy balance and the fraction contributed by the powder. After all, in an ideal PTA process, nearly all energy goes into the powder whereas the base metal is only molten on a thin surface layer-just enough to make the coating "stick".

6 List of symbols

B	magnetic induction
F, **f**	force
g	gravity
I	momentum of inertia
j	current density
p	pressure
v	velocity
u	internal energy

$\dot{\mathbf{q}}$	energy source term
S_h	heat source
$\mathbf{T}$	torque
$\mathbf{x}$	position
ρ	density
σ	conductance
τ	shear stress
ω	angular momentum

References

Ansar, S. A. (2004): *Co-projection d'alumine et d'acier inoxydable par plasma arc*. PhD thesis, GIK Institute of Engineering Sciences & Technology and the Universite de Limoges, 2004.

Bach, F.-W.; Möhwald, K.; Rothardt, T.; Prehm, J.; Engl, L.; Hartz, K.; Drößler, B. (2004): Particle Image Velocimetry in thermal spraying. *Material Science and Engineering A*, vol. 383, pp. 146–152.

Boulos, M.I.; Fauchais, P.; Pfender, E.. *Thermal Plasmas*, volume 1.

Bird, R.B.; Stewart, W.E.; Lightfoot, E.N.. *Transport Phenomena*. John Wiley & Sons.

Fluent 6.2 User's Manual, 2005.

Gonzales, J. J.; Lago, F.; Freton, P.; Masquere, M.; Franceries, X. (2005): Numerical modelling of an electric arc and its interaction with the anode: part II. The three-dimensional model–influence of external forces on the arc column. *Journal of Physics D: Applied Physics*, vol. 38, no. 2, pp. 306–318.

Ikeda, Y.; Yamada, N.; Nakajima, T. (2000): Multi-intensity-layer-particle-image velocimetry for spray measurements. *Measurement Science and Technology*, vol. 11, pp. 617–626.

Jankovic, M. M. (1997): *Study of Atmospheric Plasma Spray Process with the Emphasis on gas shrouded nozzles*. PhD thesis, University of Toronto, 1997.

Kucuk, A.; Lima, R. S.; Berndt, C. (2001): Influence of Plasma Spray Parameters on In-flight characteristics of ZrO_2-8 Wt% Y_2O_3 ceramic particles. *Journal of the American Ceramic Society*, vol. 84, no. 4, pp. 685–692.

Murphy, A.; Arundelli, C. (1994): Transport coefficients of argon, nitrogen, oxygen, argon-nitrogen, and argon-oxygen plasmas. *Plasma Chemistry and Plasma Processing*, vol. 14, no. 4, pp. 451–490.

Vardelle, M.; Vardelle, A.; Fauchais, P.; Moreau, C. (1994): Pyrometer system for monitoring the particle impact on a substrate during a plasma spray process. *Measurement Science and Technology*, vol. 5, pp. 205–212.

Wesling, V.; Giese, P. (2006): Experimental and numerical determination of the behaviour of particles during plasma transferred arc welding. *Steel Grips*.

Zscheztsche, J.; Füssel, U.; Schnick, M.; Zosel, J.; Guth, U.; Dörner, K. (2005): Strömungsmessungen im Schutzgasfreistrahl beim Lichtbogenschweißen. *Schweißen und Schneiden*, vol. 11, pp. 638–643.